communications earth & environment

ARTICLE

https://doi.org/10.1038/s43247-023-00709-5 OPEN

Dating mylonitic overprinting of ancient rocks

Christopher L. Kirkland[1✉], Hugo K. H. Olierook[1,2], Martin Danišík[2], Janne Liebmann[1], Julie Hollis[3,4], Bruno V. Ribeiro[1] & Kai Rankenburg[2]

Deformation in shear zones is difficult to date because mylonites can preserve partially reset pre-existing isotopic signatures. However, mylonites can be key structural elements in terrane recognition, so an accurate estimation of their age is important. Here we determine the in situ Rb–Sr isotopic composition of mica from major NE-SW trending mylonitic zones in the Archean Akia Terrane of Greenland and complement this information with inverse thermal history modelling. Rb–Sr isochrons indicate a dominant age of radiogenic-Sr accumulation in biotite of around 1750 million years (Ma) ago. Yet, magmatic titanite is unreset yielding a U–Pb age of around 2970 Ma. These constraints require that biotite Rb–Sr directly dates mylonitic fabric generation. The 1750 Ma mylonites, associated with the Proterozoic Nagssugtoqidian Orogeny, overprint Archean crust widely regarded as preserving evidence of early Earth horizontal tectonics.

[1] Timescales of Mineral Systems Group, School of Earth and Planetary Sciences, Curtin University, Perth, Australia. [2] John de Laeter Centre, Curtin University, Perth, Australia. [3] EuroGeoSurveys, Rue Joseph II 36-38, 1000 Brussels, Belgium. [4] Department of Geology, Ministry of Mineral Resources, Government of Greenland, P.O. Box 930 Nuuk, Greenland. ✉email: c.kirkland@curtin.edu.au

Terranes are discrete areas of crust with distinct tectonostratigraphic characteristics, separated by shear zones[1]. The crust enclosed within the bounding shear zones represents disparate continental lithosphere brought together with other distinct crustal elements only later in its evolution. The recognition of terranes is critical in understanding the geological evolution of a region. In particular, Archean terranes may provide fundamental evidence for the switch from dominantly vertical (i.e., stagnant-lid) to horizontal (plate) tectonic processes. One such area where the terrane concept has been highly important in developing models of crustal evolution is in the North Atlantic Craton of West Greenland. Later in the history of an assembled mosaic of terranes, far-field effects of distant plate reorganizations may be important. Such distal forces may reactivate ancient favorably orientated fabrics and also generate new structures. The effects of intra-continental tectonics could be expected in all terranes that went through a mobile-lid stage, regardless of their age. This process is examined in the Archean Akia Terrane.

Mylonites reflect zones of high-strain rate where dominantly ductile deformation at variable temperatures has been localized either along terrane boundaries or along later dislocations within a single terrane. These zones of ductile flow may thus provide key evidence for the kinematics and structure of an orogen and help with the understanding of far-field effects in stable crust. Accurate dating of mylonitization has been a repeated goal in the geosciences, with a wide range of approaches including, among others, thin slab whole rock Rb–Sr dating[2], K-Ar microstructurally-constrained and bulk fault gouge dating[3], and Ar-Ar dating of neocrystallized fault related phyllosilicates[4]. However, in some cases results have been difficult to interpret, due to the heterogeneous composition of mylonites containing both deformed relict porphyroclasts, as well as newly crystallized grains. Furthermore, mylonites provide pathways that localize fluids and secondary alteration. As each of the aforementioned geochronological techniques require sample disaggregation, inadvertent physical mixtures of different mineral generations can yield ambiguous mixed ages that fail to accurately capture the timing of geological events, including shearing. Consequently, mylonite dating has been described as one of the most difficult problems in geochronology[5].

Southern West Greenland hosts the North Atlantic Craton, retaining a crustal history from at least 3.8 Ga. This region represents one of the largest, best exposed, tracts of Archean crust on Earth[6]. The craton extends west into Canada[7] and east into southeastern Greenland[8] and north western Scotland[9]. In Greenland, the North Atlantic Craton comprises several terranes, including the Akia Terrane, north of Nuuk city, which is a volumetrically large component and cut by various mylonites (Fig. 1). The Akia Terrane consists mainly of igneous rocks which crystallized at c. 3230–3190 Ma and 3070–2970 Ma[1,10,11], with the latter being much more voluminous. This c. 3000 Ma Mesoarchean magmatism was coeval with high temperature, low pressure granulite-facies metamorphism[12,13]. On the northern side of the Akia Terrane 2877–2857 Ma supracrustal rocks are preserved within the Alanngua Complex[14]. These supracrustal rocks were deposited onto a Mesoarchean basement[15], buried to >30 km depth, and partially melted, during regional high-grade metamorphism between 2857 and 2700 Ma[16]. Apatite Sm–Nd and Lu–Hf isochrons at c. 2700 Ma from the Akia Terrane, indicate pervasive isotopic re-equilibration also occurred during this event[17]. This Neoarchean metamorphism, which occurred alongside the Akia Terrane margin, is akin to that in adjoining terranes, indicating a shared history of thermal disturbance. Furthermore, such commonality implies these crustal elements were linked at least by this time[14,15]. Subsequent lower grade (greenschist- to amphibolite facies) c. 2630 Ma and 2540 Ma metamorphism is evidenced by metamorphic zircon overgrowths and neoblastic apatite[18] and titanite[19], respectively. Foundational Rb–Sr work in the 1970's and 1980's in the North Atlantic Craton was interpreted to reflect loss of radiogenic-Sr in biotite from regions south of the Akia Terrane, including the Godthaabsfjord and Isukasia areas at 1700–1600 Ma[20,21]. It is unclear whether these results reflect any new fabric generation or solely isotopic resetting.

Here with the use of thermal history modeling, we seek to link isotopic ages of minerals in the Archean Akia Terrane of South West Greenland to their growth mechanism and ultimately date structures. We present a case study from four adjacent, subparallel, mylonite zones, linked to NE-SW trending sub-vertical terrane boundary parallel faults. We employ in situ biotite Rb–Sr geochronology via laser ablation triple quadrupole inductively coupled plasma mass spectrometry (QQQ-ICPMS) that permits the efficient direct analysis of texturally controlled phyllosilicate minerals linked to the mylonite fabric. We supplement this isotopic data with titanite U–Pb geochronology to evaluate the higher temperature history of these rocks and integrate these results to develop a coherent thermal evolution model to address the timing of mylonite formation. Our findings highlight the effects of the c. 1910–1770 Ma Nagssugtoqidian Orogeny, south of the inferred orogenic front, and caution about the assumption that all structures are Archean in this region.

Results

Four samples along regionally important NE-SW striking shear zones and one sample from an unfoliated granite were selected for geochronology (Fig. 1). All samples were analyzed directly on standard petrographic polished thin sections (Fig. 2).

Rb–Sr. Sample 1276; Tonalite: This sample of mylonitic tonalite was collected from a major NE-striking shear zone (Ilivilik Shear Zone), southeast of the Qaqarssuk carbonatite, 2.5 km east of Qoorupiluup Tasia. The shear zone has more than 50 km strike length and a variable width of up to 100 m. The sample is from within the Fiskefjord Complex. A proximal sample of an associated pegmatitic component of the intrusive complex yielded a 3009 ± 4 Ma zircon U–Pb crystallization age (Sample 1036[22]). The tonalite has a heterogeneous texture varying from protomylonite to ultramylonite on the outcrop scale. The sample consists of 50% plagioclase, 23% quartz, 15% biotite, 5% K-feldspar, and accessory augite, calcite, magnetite, titanite, sericite, apatite, amphibole, and zircon (Fig. 2). Plagioclase porphyroclasts are surrounded by a network of quartz. Quartz is medium- to coarse-grained typically displaying undulose extinction, irregular to serrate grain boundaries suggesting recrystallization via subgrain rotation. Plagioclase twinning is rarely bent indicating incipient crystal-plastic deformation. Fine-grained biotite defines high-strain layers (C structures) establishing the mylonitic foliation, whereas medium-grained biotite is commonly associated with S structures, linking it to shearing deformation. Biotite is more prevalent in strain shadows of plagioclase porphyroclasts and also fills rare extensional fissures within the plagioclase, oriented at a high angle to the foliation. Apatite grains are located in the quartz network and are dominated by small euhedral prisms. Titanite is generally medium-grained, subhedral, fractured and oriented parallel to the mylonitic foliation, implying it behaved as a rigid porphyroclast. Forty-nine spot analyses on biotite yield a Rb–Sr isochron age of 1773 ± 12 Ma, with an initial $^{87}Sr/^{86}Sr$ of 0.7027 ± 0.0042 (MSWD = 0.6; Fig. 3), interpreted as the best estimate of the time of biotite Rb–Sr closure to radiogenic-Sr diffusion. No spatial variation in biotite apparent ages is evident.

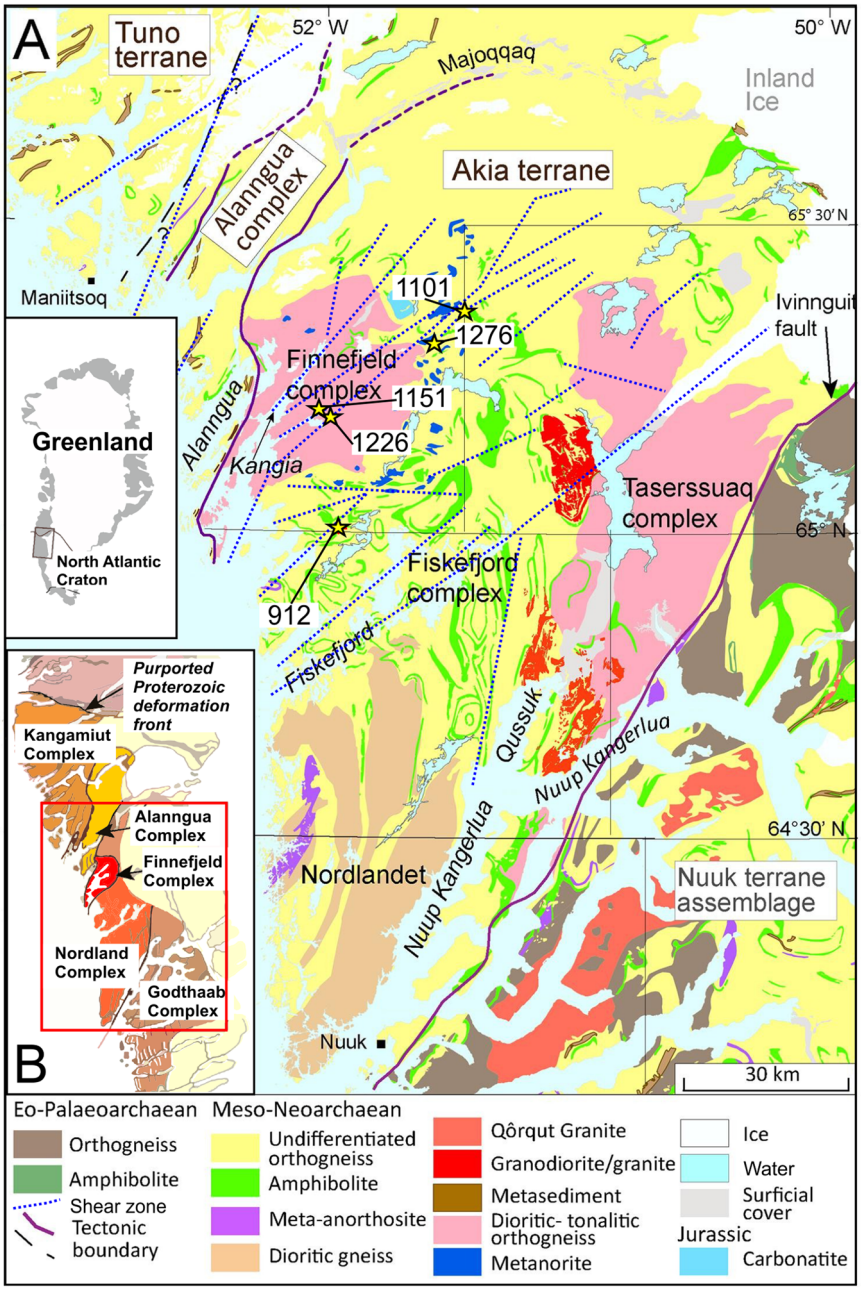

Fig. 1 Schematic geological map of South West Greenland and geographic context of the study region. A Lithological units within the Nuuk-Maniitsoq region[14,69]. Blue dashed lines are major faults inferred from aerial photography. Yellow star symbol denotes sample locations. **B** Major lithotectonic units/terranes in the region.

Sample 1226; Felsic gneiss: This mylonitic felsic gneiss was sampled near Puiattoq and is within the Finnefjeld Complex. Also sampled from the Ilivilik shear zone in a location where the mylonitic shear zone is more than 10 meters wide. A proximal dioritic gneiss sample yielded a 2998 ± 6 Ma zircon U–Pb crystallization age[23]. The sample consists of 44% plagioclase, 18% K-feldspar, 13% quartz, 12% biotite, 7% muscovite, and accessory titanite, augite, apatite, clay, zircon, amphibole, allanite, epidote, and chlorite (Fig. 2). K-feldspar and quartz are dominantly within veins consistent with an early in situ melt genesis. Texturally, the rock is protomylonitic. Quartz is generally elongated with oblique grain-shape preferred orientation, displays undulose extinction, irregular to straight grain boundaries, and chessboard textures suggesting recrystallization via subgrain rotation. Biotite and muscovite are generally oriented parallel to the mylonitic foliation and well-developed S/C structures, linking them to shearing deformation. Epidote (zoisite and clinozoisite) is common throughout the rock, rarely as syn-kinematic mega-crysts, likely suggesting fluid percolation during shearing deformation. Forty-eight biotite spot analyses yield an overly dispersed errorchron age of 1523 ± 150 Ma, with geologically meaningless negative initial $^{87}Sr/^{86}Sr$ of −0.34 ± 0.44 (MSWD = 85). The scatter of these data and the initial $^{87}Sr/^{86}Sr$ indicate this biotite has undergone secondary alteration that has modified the Rb–Sr systematics. Individual biotite model ages (calculated as two-point isochrons pinned to an average crustal initial $^{87}Sr/^{86}Sr$ of 0.715 ± 0.015), yield apparent ages of c. 1650 to c. 750 Ma, the oldest of which may best reflect the minimum time through Sr isotope diffusion for the primary biotite. A correlation is apparent between ablation spot petrology and apparent age, where younger

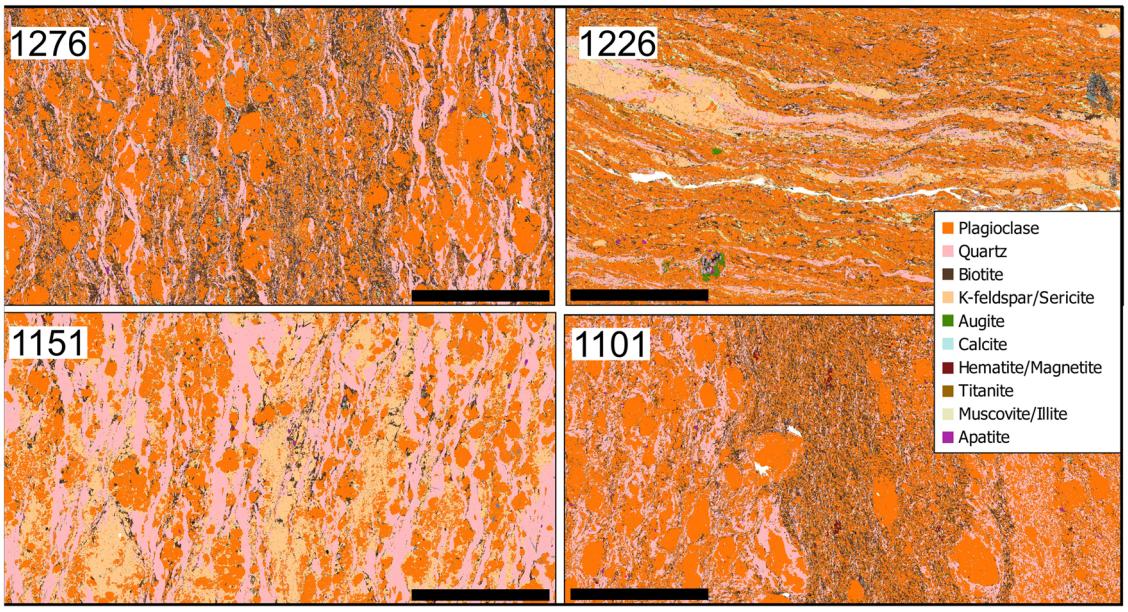

Fig. 2 False color mineral maps of Akia Terrane mylonites. Tescan TIMA mineral identification images of thin sections from various mylonites in tonalite and felsic gneiss, Akia Terrane, Greenland. The black bar in each thin section image denotes a 10 mm scale.

apparent ages are associated with a greater area percentage of a Fe- and Mg-poor alteration product of biotite, as visible in BSE images (Fig. 4). Fifty muscovite spot analyses yield a slightly overdispersed errorchron age of 1627 ± 20 Ma, with initial $^{87}Sr/^{86}Sr$ of 0.7141 ± 0.0063 (MSWD = 5.7; Fig. 3), interpreted as a minimum age estimate on the time of closure to Sr diffusion in muscovite. Muscovite and high Rb/Sr biotite ($^{87}Rb/^{86}Sr > 400$), inferred as least altered, yield an errorchron age of 1622 ± 18 Ma, with initial $^{87}Sr/^{86}Sr = 0.7147 \pm 0.0006$ (MSWD = 5.2; Fig. 3), interpreted as the best estimate of the minimum age of closure to Sr diffusion in most grains. The most radiogenic biotite analysis yields a comparable model age of 1648 Ma. If a $^{87}Sr/^{86}Sr$ of 0.715 is a reasonable estimate for the initial Sr reservoir altered biotite equilibrated with, then alteration occurred at some time after c. 800 Ma.

Sample 1151; Felsic gneiss: This mylonitic tonalitic gneiss sample, of the Finnefjeld Complex, was recovered from Qooqqut Naerlunnguat. Sampled from a steeply dipping NE-striking mylonitic shear zone with at least 15 km strike length and width (at sample location) of more than 100 m. The outcrop comprises mylonitic tonalitic to dioritic gneisses with compositional layering, isoclinal folding and (locally) dextral shear sense indicators. The outcrop consists of variably sheared and intermingled tonalite, granodiorite, and diorite, with amphibolite boudins. A c. 568 Ma kimberlite dyke intrudes in close proximity to this outcrop and c. 3006 Ma dioritic gneisses have been dated 7 km west of this locality[24]. The sample comprises 43% plagioclase, 26% quartz, 18% K-feldspar, 8% biotite, 4% muscovite, and accessory minerals include apatite, augite, titanite, allanite, and calcite (Fig. 2). Quartz grains display elongate ribbons with oblique grain-shape preferred orientation, undulose extinction, and serrate grain boundaries, typical of recrystallization via grain boundary migration. Newly formed fine-grained and sub-rounded (equant) quartz grains along the boundaries of large quartz crystals may indicate lower-grade microstructural superposition during retrograde metamorphism/deformation, likely due to quartz recrystallization via subgrain rotation or bulging. Biotite vary in grain size (from fine- to medium-grained) and define discrete S/C structures linking this mineral to shearing deformation. Fifty-three biotite spots yield a slightly over-dispersed errorchron age of 1738 ± 19 Ma, with initial $^{87}Sr/^{86}Sr$ of 0.683 ± 0.058 (MSWD = 3.1; Fig. 3). Biotite model ages, defined through the initial $^{87}Sr/^{86}Sr$ from the regression, yield a prominent apparent age peak at c. 1750 Ma. A spatial relationship between the petrographic texture in the ablation locations and their apparent ages is hinted at. Patches of the thin section with a generally smaller grain size and granular texture, appear on average to have younger apparent ages (e.g., potentially a result of minor radiogenic-Sr loss), consistent with the slight over-dispersion on the regression fit.

Sample 1101; Felsic gneiss: This mylonitic felsic gneiss sample from the Fiskejord Complex was recovered from just south of Sillisissannguit Tasiat, and about 2 km east of a major mapped NE-striking fault. Sampled from a steeply dipping NE-striking mylonitic shear zone, subparallel to the Ilivilik shear zone within the Fiskefjord Complex, but to the SE. This shear zone has a strike length of at least 10 km and is several tens of meters wide. The outcrop consists of variably sheared tonalite, granodiorite, and diorite, with pods of norite. The sample comprises 34% quartz, 33% plagioclase, 25% K-feldspar, 3% biotite, and accessory muscovite, apatite, augite, rutile, and calcite (Fig. 2). The sample is compositionally banded with a finer-grained lepidoblastic domain dominated by biotite, whereas the granoblastic domain is quartz-rich with fine-grained biotite commonly pinning quartz microstructures. Plagioclase forms porphyroclasts defining a protomylonitic texture. Quartz grains from both domains displays undulose extinction, irregular to straight grain boundaries, and chessboard textures, suggesting recrystallization via subgrain rotation. In the lepidoblastic domain biotite defines well-developed S/C structures linking it to shearing deformation. Thirty-eight biotite spot analyses yield an isochron age of 1746 ± 18 Ma, with initial $^{87}Sr/^{86}Sr$ of 0.7102 ± 0.0038 (MSWD = 0.6; Fig. 3).

Sample 912; Granite: This weakly foliated granite sample from the Fiskejord Complex was taken from just south of Annikitsoralak, and adjacent to a NE-SW elongated lake. The outcrop consists of a layer of isoclinally folded granite that is in contact with amphibolite. The sample comprises 45% K-feldspar, 33% quartz, 21% plagioclase, and accessory muscovite, magnetite, chlorite, and zircon (Fig. 5). Muscovite in this sample is very fine-

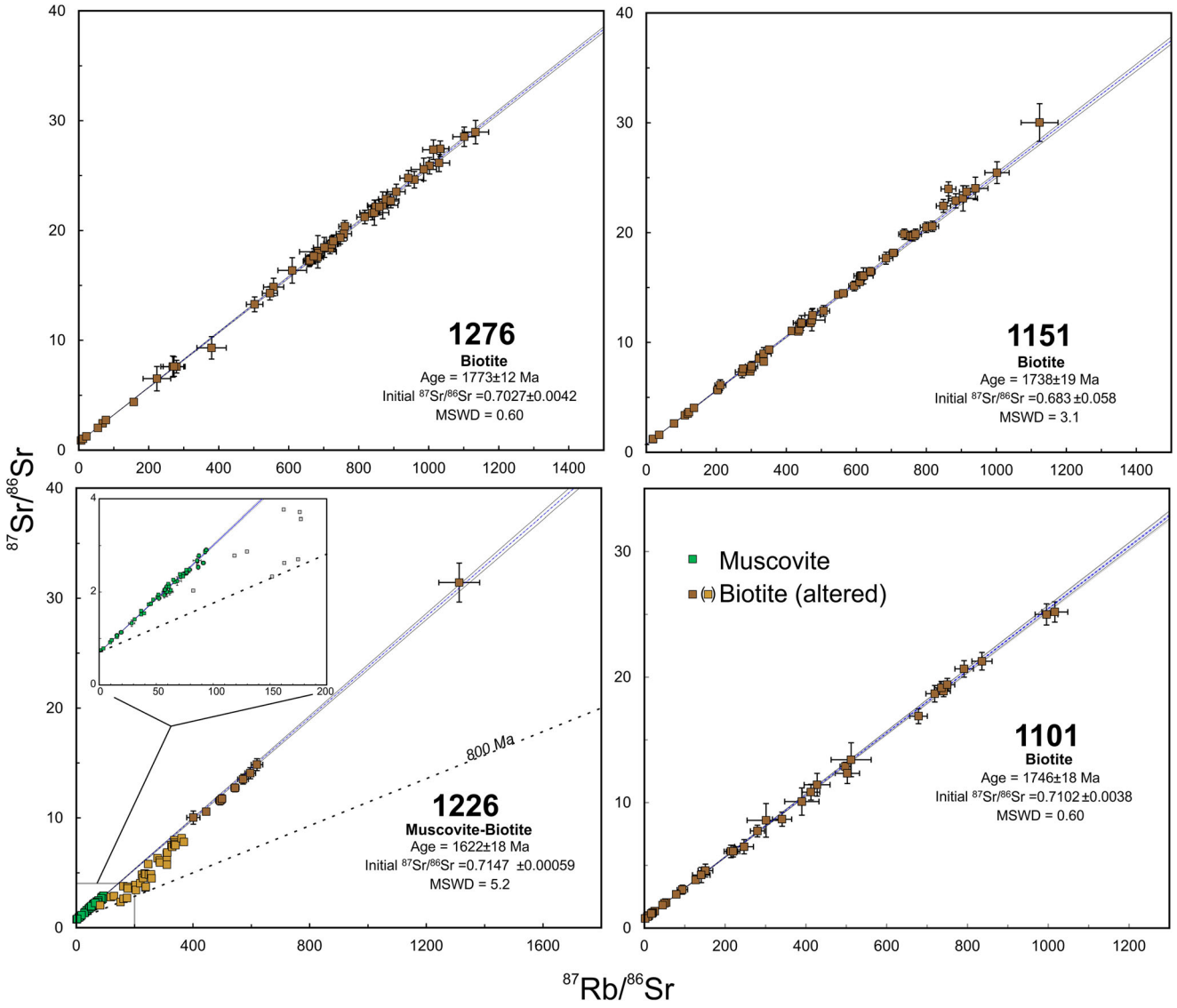

Fig. 3 Rb–Sr isochron diagrams. Rb–Sr biotite (muscovite) isochron diagrams for mylonites, Akia Terrane, Greenland. Each panel contains the isotopic results from one sample as indicated by the sample number in the lower right of each plot. Error bars are shown at the two-σ level. Uncertainties around the regressions are at the 95% confidence level.

grained (usually <10 μm) and is present as inclusions in K-feldspar (e.g., sericite). Twelve spots on muscovite (plus inevitable K-feldspar mixtures) yield an errorchron of 2369 ± 200 Ma, with an initial $^{87}Sr/^{86}Sr$ of 0.786 ± 0.0098 (MSWD = 20; Fig. 5). The initial ratio is much greater than in typical Archean crust and implies variable rejuvenation with a radiogenic metamorphic Sr reservoir, consistent with the scatter from an isochron.

U–Pb and trace elements. Titanite in the mylonitic tonalite sample 1276 occurs as individual blocky grains or as grain aggregates. The latter may be displaced with accompanying grain size reduction within the ductile shear fabric (Fig. 6). Sixty-one analyses define a mixing line between radiogenic and common Pb components, with the upper intercept implying a common $^{207}Pb/^{206}Pb$ of 0.949 ± 0.074 with a lower intercept age of 2941 ± 39 Ma (MSWD = 4.4; Fig. 7). The MSWD indicates that there is scatter greater than analytical uncertainties alone, with individual ^{207}Pb-corrected ages (assuming 2940 Ma common Pb after ref. [25]) ranging from 3375 Ma to 2884 Ma with a unimodal peak at 2999 Ma with low excess kurtosis (3.2), implying a distribution deviating slightly from normal. Common Pb (as estimated by $f207\%$) varies from 0 to 58%. Excluding two analyses that may have hit inclusions or epoxy and 18 analyses lying to the right of the regression that have faded internal BSE textures indicative of minor radiogenic-Pb loss, the remaining analyses yield a regression that intersects the concordia at 2971 ± 28 Ma (MSWD = 1.3; $n = 40$).

Titanite trace element content may differentiate between magmatic, recrystallized, and metamorphic growth[26]. A titanite chondrite-normalized rare earth element (REE) plot of analyses from sample 1276 reveals fractionated patterns dominated by light-REE with an average $(La/Lu)_N$ of 6.87 and generally a positive Eu anomaly (Fig. 8). Using shape coefficients to mathematically compare chondrite-normalized REE patterns[27], we conclude that this titanite is igneous (Fig. 8). Other trace element signatures such as Th/U (average of 1.44) and Th/Pb (average of 2.86) also support an igneous origin for this mineral[28,29]. Zr-in-titanite temperatures[30] imply temperatures of ~770 °C for crystallization, assuming a zircon-quartz buffered system at 0.8 GPa[16].

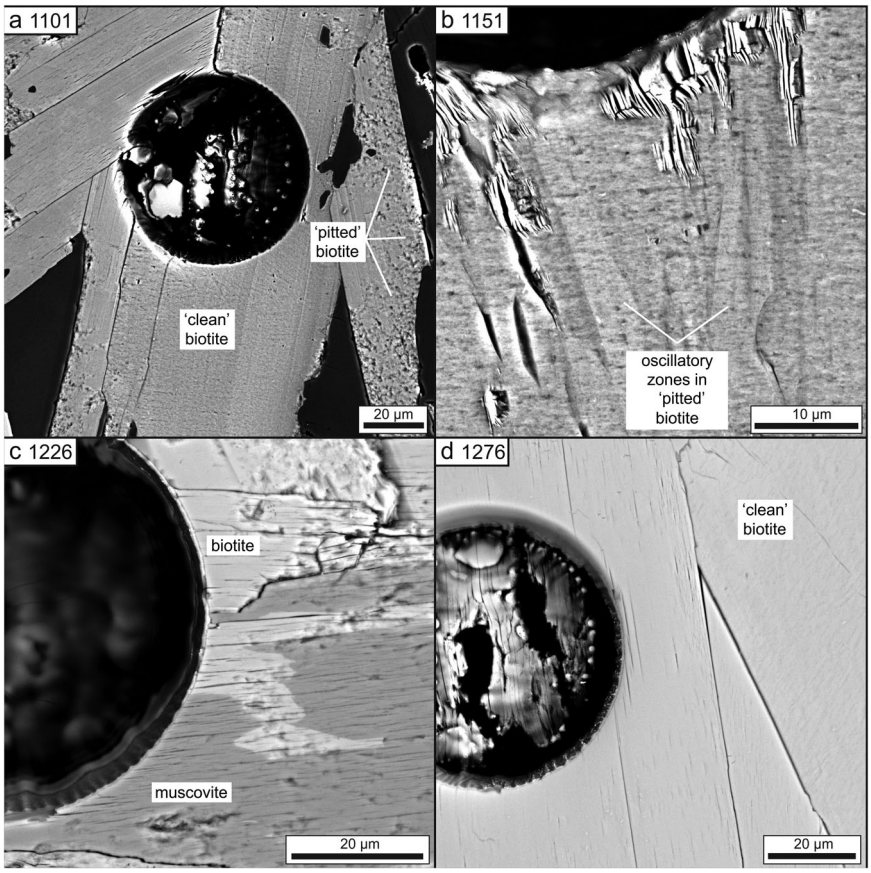

Fig. 4 Representative backscatter electron images of mica grains. Different mica grains within samples analyzed for Rb-Sr geochronology with various portions of laser ablation sample pits are shown. Each representative image contains the corresponding sample number in the upper left of each panel.

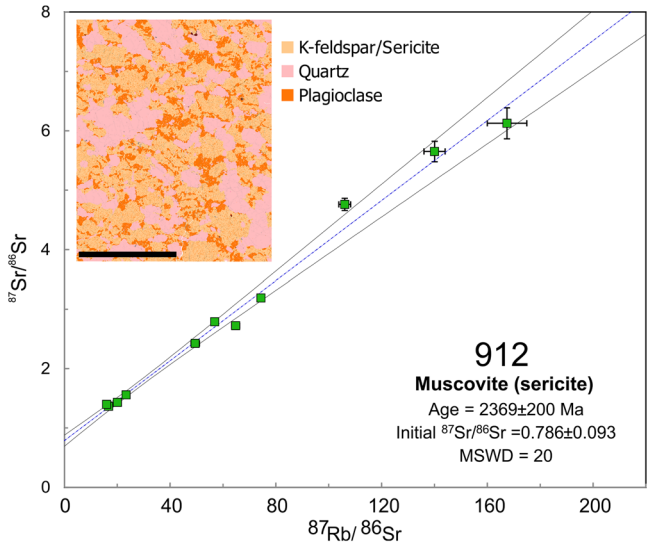

Fig. 5 Rb-Sr muscovite isochron diagram. Isochron for unfoliated granite sample 912 Akia Terrane, Greenland. Error bars are shown at the two-σ level. Uncertainties around the regressions are at the 95% confidence level. Inset shows a false color mineral map of the sample thin section, with the black bar denoting a 10 mm scale.

Discussion

Mica ages. Violin plots of biotite Rb–Sr model ages can be constructed (Fig. 9), assuming an initial $^{87}Sr/^{86}Sr$ constrained by the intercept of the least squares regression in each sample, provides a reasonable indication of the Sr isotopic reservoir with which the biotite equilibrated. Notably, there is low sensitivity in calculated age to the choice of initial $^{87}Sr/^{86}Sr$ ratio given the highly radiogenic biotite $^{87}Sr/^{86}Sr$ ratios[31]. Biotite model ages for three of the four mylonite samples cluster at c. 1750 Ma, with one sample associated with altered biotite (Fig. 4), showing a greater spread from Paleoproterozoic to Neoproterozoic apparent ages.

Empirical field-based studies in Europe have implied Rb–Sr closure temperatures of ~300 °C in biotite and ~500 °C in muscovite[32]. Muscovite from sample 1226 with altered biotite indicates Rb–Sr apparent dates around c. 1615 Ma that contrast with highly dispersed and seemingly younger biotite apparent model ages. Muscovite in sample 1226 lacks obvious alteration, whereas biotite in places has intergrowths of a lower Mg- and Fe-mica secondary reaction product (Fig. 4). The commonly reported closure temperatures for the Rb–Sr geochronometer in muscovite is in the range of 500 °C to >600 °C[33], yet it has been proposed that muscovite can lose Sr due to deformation at temperatures <500 °C[34]. Furthermore, mineral composition has also been linked to variable Sr retention[35]. In contrast to the more consistent muscovite ages in sample 1226, the distribution of apparent ages in biotite implies a secondary alteration that has partially rejuvenated its Sr isotopic composition. Nonetheless, most samples show well-defined biotite isochrons with estimates of model ages clustering at c. 1750 Ma (Fig. 9).

Given these data, an important question to address is how closely the biotite Rb–Sr ages of c. 1750 Ma approximate the growth age of the shear zone fabric. In other words, did biotite grow prior to c. 1750 Ma, above its Sr closure temperature, and did the mylonites only cool at this time? To address this question

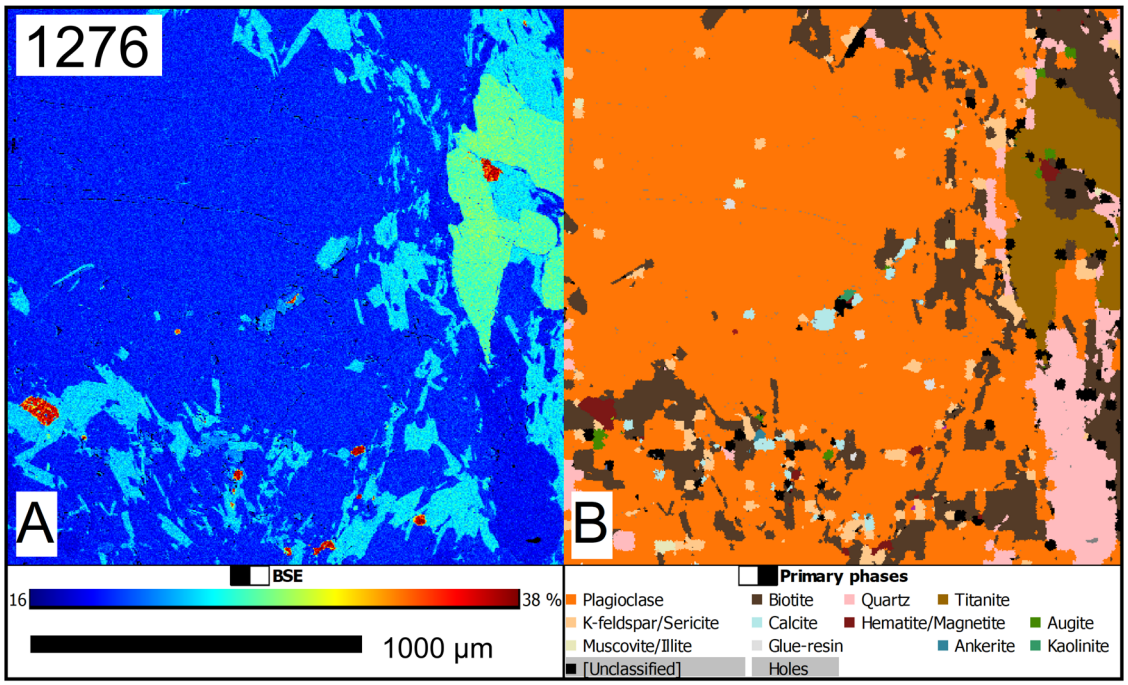

Fig. 6 Representative images of Akia Terrane tonalite containing titanite. A False color backscatter electron (BSE) image of sample 1276, Tonalite, showing titanite (green). False color gradient scale bar denotes BSE intensity. The red minerals denote Fe oxide phases. **B** phase map of the same region.

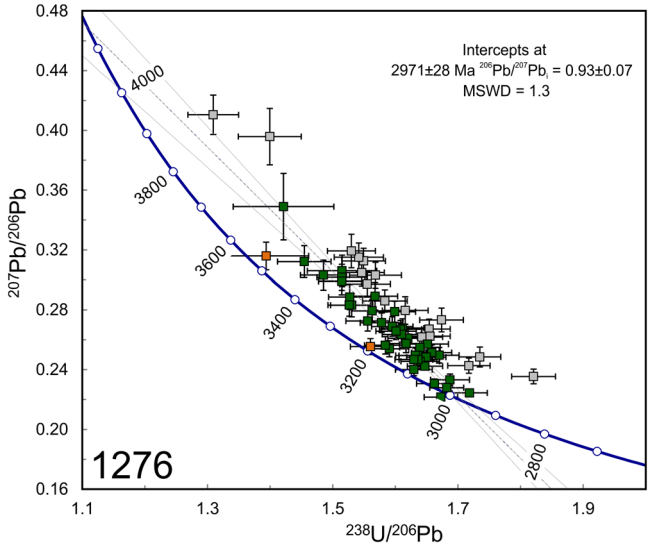

Fig. 7 Tera-Wasserburg Concordia diagram of titanite from sample 1276. Green squares denote main group, gray squares denote potential minor radiogenic-Pb loss, and orange squares denote potential old outliers/ analytical mixtures with epoxy. Error bars are shown at the two-σ level. Uncertainty around the regression line is shown at the 95% confidence level.

we first need to consider the highest temperature that these rocks experienced.

Primary magmatic temperatures of these TTG are likely around ~750–800 °C[16] and, depending on the overprinting history, the titanite U–Pb system could retain its primary magmatic crystallization age if it reflects an igneous mineral. Despite a slight skewness towards younger ages, the titanite U–Pb age distribution is broadly consistent with a single age component with only minor radiogenic-Pb loss or perhaps a slight closure temperature differential in the grain population. The dominant titanite U–Pb age of c. 2970 Ma is similar to the c. 3000 Ma zircon U–Pb magmatic crystallization age for Akia Terrane felsic gneisses[24]. Trace element patterns of this titanite are also characteristic of a magmatic genesis and the Zr concentration supports a magmatic crystallization temperature of ~770 °C. Both the U–Pb systematics and REE compositional pattern point to magmatic titanite growth during the main regional magmatic emplacement event[24], which dominated the isotopic memory of this mineral, with subsequent thermal conditions being unable to wholesale reset its U–Pb system.

Whilst high-temperature granulite-facies conditions have been established for parts of the Akia Terrane in its early history (western Fiskefjord complex and southern Alanngua complex), other regions within the terrane only reached amphibolite facies conditions[14,16,36]. A subsequent Late Mesoarchaean to Neoarchaean (2857–2700 Ma) granulite-facies metamorphic overprint (~820–850 °C at 8–10 kbar) was reached in the Alanngua complex[14] but clearly cannot have pervasively affected the area around sample 1276, as its titanite U–Pb age is not strongly affected by thermally activated diffusive radiogenic-Pb loss post-magmatic crystallization.

With the higher temperature conditions evaluated, we can now better understand the meaning of the biotite Rb–Sr data. We employed inverse thermal history modeling (Supplementary Figure 2) to test whether the measured biotite Rb–Sr dates represent the time of biotite formation/crystallization (i.e., biotite Rb–Sr dates are crystallization ages of newly formed biotite), or record cooling of pre-existing biotite after an earlier metamorphic peak (i.e., biotite Rb–Sr dates are cooling ages; Fig. 10).

To test these hypotheses, we first constrained the maximum temperatures the samples could have experienced during the time recorded by the biotite Rb–Sr data (i.e., c. 1750 Ma) by utilizing the titanite U–Pb data. Maximum temperatures were modeled based on available titanite U–Pb ages clustering at 2970 Ma and the experimentally determined diffusion kinetic parameters for the titanite U–Pb system ($E_a = 328.7$ kJ mol^{-1} and $D_0 = 0.001$ cm^2 s^{-1})[37]. The modeling results suggest that the

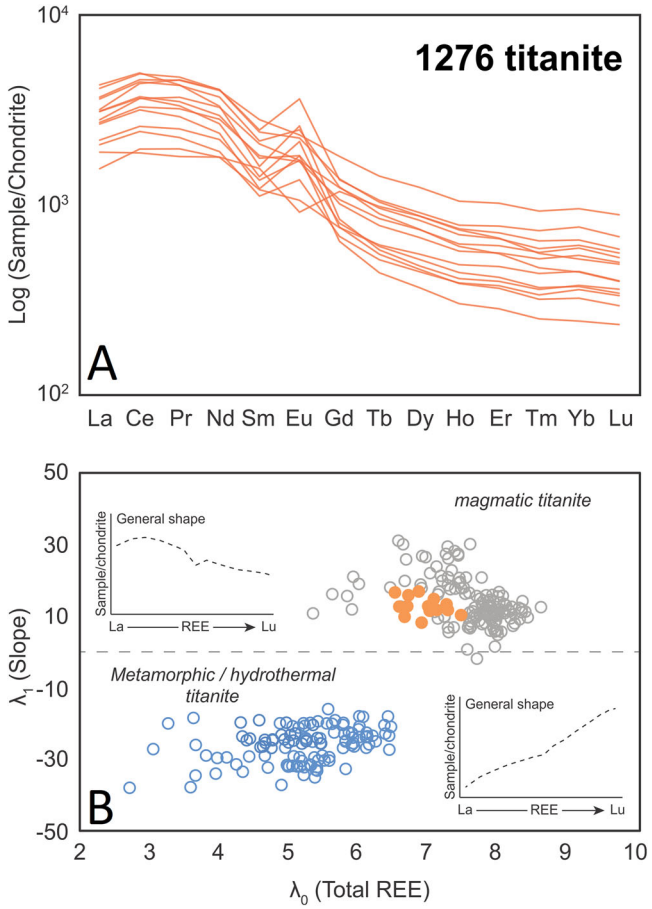

Fig. 8 Titanite trace element geochemistry. A Titanite chondrite-normalized REE patterns from sample 1276 using reference values from ref. [70]; **B** Comparison between sample 1276 titanite (filled orange circles) and typical magmatic (gray unfilled circles) and metamorphic titanite (blue unfilled circles) compiled from the literature[27]. The reader is referred to ref. [71] for information about the lambda (λn) parameters, which were calculated using BLambdaR[72].

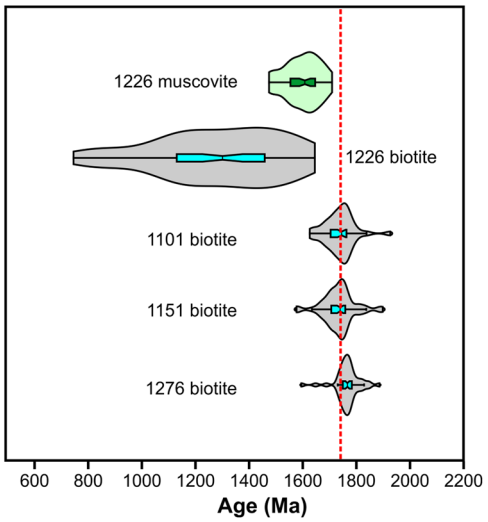

Fig. 9 Measures of central tendency and variability in Rb-Sr ages from Akia Terrane mica grains. Violin plots with box and whisker overlay of biotite and muscovite Rb-Sr model ages. Median values are denoted by the central black line in the box, Q1 and Q3 by the bars. Red vertical bar denotes mode at c. 1750 Ma. Muscovite is indicated by the green fill in the violin plot of sample 1226.

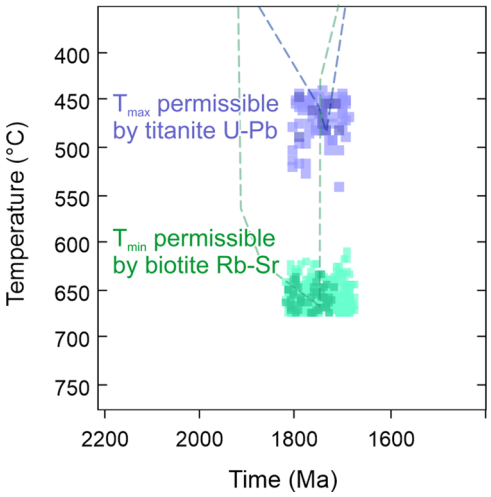

Fig. 10 Time-temperature evolution models. Thermal history models constrain the maximum permissible temperature to leave titanite unreset (blue squares) yet entirely thermally reset biotite (green squares). The difference in calculated temperature implies that biotite Rb-Sr reflects a neoblastic age.

maximum permissible temperatures at 1750 ± 68 Ma recorded by the biotite Rb–Sr data could not exceed ~530 °C, otherwise the titanite would not have been able to retain its U–Pb igneous crystallization signature. Whilst a wide range of Pb diffusion parameters exist for titanite[38], with some equivalent to diffusion rates of Sr in titanite[39], variation to coefficients within plausible ranges make little difference to the conclusion that biotite temperatures cannot have greatly exceeded ~500–550 °C (Fig. 6).

In the second model, we aimed to constrain the maximum temperature at c. 1750 Ma by utilizing the biotite Rb–Sr model age and grain size data. The biotite grains range in size from ~5 to ~600 µm in diameter (Supplementary Data 6), nevertheless the measured (>64 µm) biotite Rb–Sr dates tends to form tight clusters (c. 1750 Ma) regardless of the grain size. To incorporate this observation into the model, we computed thermal trajectories simultaneously for diffusion domains of different sizes (i.e., 10, 50, 100, 200 µm in diameter), adopting diffusion kinetic parameters for biotite Rb–Sr of $E_a = 328.7\ kJ\ mol^{-1}$ and $D_0 = 0.001\ cm^2\ s^{-1}$, with the rock cooling from above the Sr blocking temperature[40]. The maximum temperatures permissible for the observed biotite Rb–Sr age and diffusion domain size are modeled to be in excess of ~610 °C. This temperature estimate on first consideration would appear to be at odds with the former model for Pb diffusion in titanite, as it would imply complete resetting of the titanite U–Pb system and hence complete rejuvenation of its U–Pb ages.

This apparent conflict between the outcomes from the two thermal history models is easily reconciled by the biotite isotopic result dating growth of this mineral at c. 1750 Ma below ~530 °C, rather than reflecting a cooling age. The fact that the biotite Rb–Sr model ages are homogeneous (and the isochrons generally rather well-defined, when not subject to secondary chemical alteration) irrespective of the biotite grain size lends additional support to a growth timing interpretation for the Rb–Sr age of biotite defining the mylonitic fabrics in these samples. A dispersed apparent age spectrum could result from slow cooling, for a biotite population of dissimilar grain sizes (e.g., >5 µm to <1 mm). Yet in the Akia Terrane mylonite data set, disparate Rb–Sr biotite ages correspond only to where petrographic

evidence of mineral alteration is detected (Fig. 4). Hence, we see no evidence of slow cooling and conclude the mylonite biotite Rb–Sr apparent age component at c. 1750 Ma is best interpreted as the time of crystallization and, thus, directly constrains the timing of mylonite generation. Furthermore, sericitic muscovite sampled from an unfoliated granite, without mylonite textures, yields a Rb–Sr errorchron of c. 2370 Ma (Fig. 5). While this age may not be directly meaningful, it necessitates regional cooling to this mineral's radiogenic-Sr retention temperature well before mylonite generation.

Strontium evolution modeling indicates that the initial $^{87}Sr/^{86}Sr$ of the Akia samples are higher than expected for average crustal Rb/Sr ratios (Supplementary Figure 3). The initial $^{87}Sr/^{86}Sr$ ratios are consistent with Sr input from a radiogenic source, either a Rb-rich crustal reservoir or metamorphic fluids (e.g., produced through devolatilization reactions[41]). U–Pb apatite ages of c. 1800–1700 Ma in the Akia Terrane have been interpreted to reflect regrowth from a compositionally distinct reservoir after primary magmatic growth, driven by regional tectonothermal and fluid activity at that time[18]. Additionally, other works on the terrane have also reported a wide range of apatite U–Pb ages between ≤3000 Ma (magmatic growth) and a dominant c. 1750 Ma (neoblastic or recrystallized) component, consistent with Proterozoic fluids partially to completely mobilizing Sr, which can be dominantly held in this mineral[17].

Regional implications. The new biotite crystallization ages at c. 1750 Ma, constraining mylonite genesis, occur in the terminal phase of the Nagssugtoqidian orogeny[42,43] and are located ~150 km south of the Nagssugtoqidian orogenic front[44]. The Nagssugtoqidian Orogen forms a Proterozoic orogenic belt the girdles the northern edge of the North Atlantic Craton and crops out in southwest and southeast Greenland[45]. The orogen includes a range of Archean and Paleoproterozoic rocks affected by polyphase deformation and high-grade metamorphism[42]. South-verging structures in its southern extent support an interpretation of subduction under the Ammassalik Intrusive Complex[46]. The southern boundary of the Nagssugtoqidian Orogen has been defined by the imprint or apparent lack thereof on Paleoproterozoic dolerite dykes[47], with the boundary of the orogen located in a near-vertical dextral shear zone[48]. However, Proterozoic thermal processes are well known from south of the Nagssugtoqidian front. For example, the Rb–Sr isotopic system of biotites in gneisses of the Godthaabsfjord region (Isukasia terrane), south of the Akia Terrane, was interpreted to reflect thermally activated resetting at 1700–1600 Ma[21]. Additionally, biotite Rb–Sr solution analyses from the Amitsoq gneisses at Isua (Isukasia terrane) yielded isochron ages of 1623 ± 65 Ma[20]. This isochron was interpreted as tracking low-grade metamorphic re-equilibration of biotite. The timing of this thermal event is also within uncertainty of a Rb–Sr age from an intrusive granite in the same region[49]. In the Akia Terrane, a c. 1690 Ma Rb–Sr two-point epidote-biotite isochron was considered to record a thermal event at that time[50].

The Nagssugtoqidian Orogen's evolution is characterized by c. 1860–1840 Ma WNW–ESE compression associated high-grade metamorphism and thrusting[51]. Subsequent c. 1775 Ma sinistral strike-slip shear zones transect the orogen[51]. Terminal Nagssugtoqidian fabrics dated by high-temperature chronometers (zircon and monazite U–Pb) yield c. 1770 Ma ages whereas amphibole $^{40}Ar/^{39}Ar$ ages of c. 1700–1740 Ma reflect cooling times during exhumation[52]. That the major NE-SW shear zone structures dipping to the northwest in the Akia Terrane have identical formation ages (as dated in this paper) to the late-stage uplift processes in the Nagssugtoqidian Orogen supports the interpretation that Proterozoic thrusts propagated southwards deep into the Archean North Atlantic Craton. This important Proterozoic orogenic overprint cautions that, despite being proposed as preserving some of the best evidence for horizontal tectonics in the Archean[53], much of the Akia Terrane, if not a larger portion of the North Atlantic Craton, was subject to subsequent structural modification, including growth of new fabrics and modification of some existing isotope systems. Biotite from further south of the Akia Terrane appears to record somewhat younger Rb–Sr isochrons of <1700 Ma[20,21,49]. These isochrons are commonly interpreted as a function of a late Proterozoic thermal overprint[21], linked to minor granitic magmatism[49]. Hence, it appears possible to distinguish between new fabric growth, in the Akia Terrane at c. 1750 Ma, coeval with epidote alteration[50], and thermal overprinting and cooling of biotite with Rb–Sr ages best estimated at c. 1620 Ma[20]. Apatite U–Pb geochronology also indicates recrystallization of this mineral at c. 1750 Ma, throughout the North Atlantic Craton[17,18,54,55].

A distinct timing of granulite-facies metamorphism affected rocks north and south of Maniitsoq, reflecting either distinct terranes, or magmatic emplacement of younger rocks to the north into an older metamorphic basement to the south[56]. The boundary along Søndre Isortoq has been envisaged as separating distinct crustal blocks (Maniitsoq in the north and Fiskefjord in the south), with different crustal levels exposed in each, which had been formed in distinct continents, and only later amalgamated by continental collision[57]. Others have proposed that this collision of the Maniitsoq block with the Fiskefjord block occurred by south-directed subduction and convergent tectonism at c. 2560 Ma[58]. Importantly, the wide commonality of Hf isotopic signatures in zircon crystals from across the North Atlantic Craton, implying a Hadean to Eoarchean crustal nucleus, indicates that crustal blocks within the North Atlantic Craton need not be disparate terranes[59]. Rather, a crustal nucleus, perhaps formed via early Earth sagduction style processes, may have been extended, fragmented, and recompressed. The imprint of several cycles of deformation, the latter of which has classic thrust geometries and mylonite zones, undoubtedly complicates the disambiguation of Archean from Proterozoic structures and confounds the distinction between horizontal and vertical plate tectonic processes in West Greenland.

Mylonitic zones in the Akia Terrane are also relevant in understanding the nature and timing of a range of later geological processes that modified the crust of this region. For example, Ni-Cu-Co mineralization in norites, which occurs in a curvilinear belt around the Alanngua fjord area, is remobilised and dissected along mylonites[60]. These norites contain semi-massive pyrrhotite-pentlandite-chalcopyrite-pyrite sulfides, with accessory magnetite and ilmenite, in brecciated units hosting rounded, centimeter-sized and larger, blocks of country rock[61]. Remobilized sulphides characteristically track into the norites and are locally associated with mylonite zones in the orthogneiss country rocks[62]. Mylonites, including one dated in this work, transect mineralized sections at Fosillik, displacing norites and remobilising the sulfide assemblage. Of note is that the greatest sulfide accumulation has been observed in proximity to the mylonite zones[62], suggesting that Proterozoic tectonism may be important in the Ni-Cu-Co ore evolution.

Additionally, the dated Akia mylonites occur in areas where cataclastic zones have been purported to relate to Earth's oldest putative bolide impact[63] (but see ref. [64]). The dating of these mylonites further calls into question the interpretation that the cataclastic zones of the region are related to a Mesoarchean impact, given that those zones have not been dated and Proterozoic deformation fabrics have now been established in the very same area.

Conclusions

Biotite Rb–Sr ages of c. 1750 Ma from mylonite fabrics in the Akia Terrane coincide with the end of the Nagssugtoqidian orogeny and highlight that structures of this age penetrate into the Akia Terrane, in line with the wide thermal halo of this event.

The dated mylonites are from amphibolite facies large shear zones, and the biotite within them grew at c. 1750 Ma rather than being reset by thermally activated volume diffusion at this time. The growth of biotite in mylonite fabrics implies that these major shear zones, which are parallel to other similar shear zones in west Greenland, including in the Nuuk region, were active at this time with fluid mobility and mineral growth.

One of the dated mylonitic shear zones cuts the Fosillik area, where Ni mineralization was remobilized along late mylonites. This suggests that Proterozoic tectonism may be important in the evolution of Ni deposits in the region.

Throughout the North Atlantic Craton Paleoproterozoic Rb–Sr mineral resetting ages are recognized. Here we show that amphibolite facies structures, in the Akia Terrane of South West Greenland, are associated with biotite growth at c. 1750 Ma. These NE-SE shear zones are south of the mapped Nagssugtoqidian deformation front. Thus, in the North Atlantic Craton there appears to be both new mineral growth on major shear zones at c. 1750 Ma, in the Akia Terrane, and also thermally activated biotite Rb–Sr resetting at a slightly later time (1700–1600 Ma), in the Isukasia terrane (e.g., ref. [21]). Such young high-grade structures and thermal effects in the North Atlantic Craton highlight that horizontal tectonics have overprinted original Archean relationships across the grain to terrane scale, accommodating unknown amounts of displacement of the stratigraphy and ultimately cautioning that interpretations of ancient geodynamics in the North Atlantic Craton, as a bastion of early Earth modern-style plate tectonics, require detailed evidence.

Methods

Mineral maps. TESCAN Integrated Mineral Analyzer (TIMA) mineral maps of thin sections (Fig. 2) were produced at Curtin University. The TIMA instrument is based around a secondary electron microscope, fusing energy-dispersive X-ray spectroscopy (EDS) and back-scattered electron (BSE) images to create mineral maps. Thin sections were carbon-coated and analysed over their full surface using a grid with 3 µm step size for BSE. A 2-µm step size was used for EDS grids or when BSE contrast changed, that is to say, when a mineral boundary was detected. EDS spectra consist of one thousand counts, are standardized to a pure Mn reference, and are statistically compared to a mineral spectra database for identification purposes. Operational conditions[65] consisted of a beam energy of 25 keV, a beam intensity of ~19 keV, a probe current of ~5.3 nA, a spot size of ~80 nm, and a nominal working distance of 15 mm. High-resolution maps of thin sections are provided in Supplementary Data 1.

Isotope analyses. All isotope measurements were carried out at the GeoHistory Facility in the John de Laeter Center, Curtin University using laser ablation techniques on polished thin sections. Rb–Sr data on biotite were collected by LA-ICPMS using a QQQ (Agilent 8900 ICPMS) with a Resonetics RESOlution SE 193 nm excimer UV laser incorporating a dual volume S155 sample cell. The 8900 was run in MS/MS mode using N_2O reaction gas. Detailed analytical procedures are provided in Supplementary Methods and all Rb–Sr data are in Supplementary Data 2. Reference biotite CK001 yielded an age of 420 ± 6 Ma ($^{87}Sr/^{86}Sr_i = 0.681 \pm 0.066$; MSWD = 0.8, $n = 53$) identical, within uncertainty, to the published value of 413 ± 3 Ma and $^{87}Sr/^{86}Sr_i$ of 0.709 ± 0.001[65,66] (Supplementary Figure 1).

Titanite U–Pb isotope (Supplementary Data 3) and trace element concentration data (Supplementary Data 4) were also obtained via LA-ICPMS analysis. Individual titanite grains were ablated utilizing a Resonetics RESOlution M-50A-LR system based on a COMPex 102 193 nm excimer UV laser. U–Pb analyses used a 5 Hz laser repetition rate with a fluence of 2.6 J cm^{-2}. The sample cell was flushed with ultrahigh purity He (350 mL min^{-1}) and N_2 (3.8 mL min^{-1}). Isotopic abundances were measured using an Agilent 8900 triple quadrupole ICPMS, utilizing high-purity Ar as the plasma gas (1 L min^{1}). The detailed LA-ICPMS method is given in the Supplementary Methods and sample geographic coordinates are provided in Supplementary Data 5.

Inverse thermal history modeling. To explore the meaning of the geochronological data (e.g., crystallization versus cooling versus partial resetting), inverse thermal history modeling using the HeFTy software[67] was employed. HeFTy reconstructs time-temperature pathways for multiple thermochronometric systems for which diffusion parameters are known or can be reasonably inferred. The specific objective of the modeling effort was to decipher the meaning of the Rb–Sr dates in biotite. Accordingly, different models were constructed as described in the following sections using grain sizes defined in Supplementary Data 6.

Data availability

All data used in this manuscript are included in the published article (and its supplementary information files). In addition, all data have been uploaded to Figshare at https://doi.org/10.6084/m9.figshare.c.5626387.v1. All isotope diagrams can be reproduced from the data uploaded to Figshare[68].

Received: 31 May 2022; Accepted: 10 February 2023;
Published online: 23 February 2023

References

1. Friend, C. R. L. & Nutman, A. P. New pieces to the Archaean terrane jigsaw puzzle in the Nuuk region, southern West Greenland: Steps in transforming a simple insight into a complex regional tectonothermal model. *J. Geol. Soc.* **162**, 147–162 (2005).
2. Maglougilin, J. F. An evaluation of Rb-Sr dating of pseudotachylyte: structural-chemical models and the role of fluids. *Geochem. J.* **37**, 21–33 (2003).
3. Scheiber, T., Viola, G., van der Lelij, R., Margreth, A. & Schönenberger, J. Microstructurally-constrained versus bulk fault gouge K-Ar dating. *J. Structural Geology* **127**, 103868 (2019).
4. Elmola, A. A. et al. 40Ar/39Ar muscovite dating of thrust activity: a case study from the Axial Zone of the Pyrenees. *Tectonophysics* **745**, 412–429 (2018).
5. Oriolo, S. et al. Geochronology of shear zones – a review. *Earth-Sci. Rev.* **185**, 665–683 (2018).
6. Friend, C. R. L., Nutman, A. P. & McGregor, V. R. Late Archaean terrane accretion in the Godthåb region, southern West Greenland. *Nature* **335**, 535–538 (1988).
7. Bridgwater, D. & Schiotte, L. The Archaean gneiss complex of Northern Labrador-a review of current results, ideas and problems. *Bull. Geol. Soc. Denmark* **39**, 153–166 (1991).
8. Kalsbeek, F. et al. Geochronology of Archaean and Proterozoic events in the Ammassalik area, South-East Greenland, and comparisons with the Lewisian of Scotland and the Nagssugtoqidian of West Greenland. *Precambrian Res.* **62**, 239–270 (1993).
9. Friend, C. & Kinny, P. A reappraisal of the Lewisian Gneiss complex: geochronological evidence for its tectonic assembly from disparate terranes in the Proterozoic. *Contrib. Mineral. Petrol.* **142**, 198–218 (2001).
10. Garde, A. A. Accretion and evolution of an Archaean high-grade grey gneiss-amphibolite complex: the Fiskefjord area, southern West Greenland. (1997).
11. Garde, A. A., Friend, C. R. L. & Nutman, A. R. & Marker, M. Rapid maturation and stabilisation of middle Archaean continental crust: the Akia terrane, southern West Greenland. *Bull. Geol. Soc. Denmark* **47**, 1–27 (2000).
12. Yakymchuk, C. et al. Reworking of the Mesoarchean crust during high-temperature–low-pressure metamorphism, Akia terrane, west Greenland. **352**, 105958 (2020).
13. Riciputi, L. R., Valley, J. W. & McGregor, V. R. Conditions of Archean granulite metamorphism in the Godthab-Fiskenaesset region, southern West Greenland. *J. Metamorph. Geol.* **8**, 171–190 (1990).
14. Steenfelt, A. et al. The Mesoarchaean Akia terrane, West Greenland, revisited: New insights based on spatial integration of geophysics, field observation, geochemistry and geochronology. *Precambrian Res.* **352**, https://doi.org/10.1016/j.precamres.2020.105958 (2021).
15. Kirkland, C. L., Yakymchuk, C., Hollis, J., Heide-Jørgensen, H. & Danišík, M. Mesoarchean exhumation of the Akia terrane and a common Neoarchean tectonothermal history for West Greenland. *Precambrian Res.* **314**, 129–144 (2018).
16. Yakymchuk, C. et al. Mesoarchean partial melting of mafic crust and tonalite production during high-T–low-P stagnant tectonism, Akia Terrane, West Greenland. *Precambrian Res.* **339**, https://doi.org/10.1016/j.precamres.2020.105615 (2020).
17. Gillespie, J. et al. Lu–Hf, Sm–Nd, and U–Pb isotopic coupling and decoupling in apatite. *Geochem. Cosmochem. Acta* **338**, 121–135 (2022).
18. Kirkland, C. L. et al. Apatite: a U-Pb thermochronometer or geochronometer? *Lithos* **318-319**, 143–157 (2018).
19. Kirkland, C. L. et al. Titanite petrochronology linked to phase equilibrium modelling constrains tectono-thermal events in the Akia Terrane, West Greenland. *Chem. Geol.* **536**, 119467 (2020).

20. Baadsgaard, H., Nurman, A. P., Rosing, M., Bridgwater, D. & Longstaffe, F. J. Alteration and metamorphism of Amitsoq gneisses from the Isukasia area, West Greenland: Recommendations for isotope studies of the early crust. *Geochim. Cosmochim. Acta* **50**, 2165–2172 (1986).
21. Pankhurst, R. J., Moorbath, S., Rex, D. C. & Turner, G. Mineral age patterns in ca. 3700 my old rocks from West Greenland. *Earth Planet. Sci. Lett.* **20**, 157–170 (1973).
22. Kirkland, C. L. et al. Theoretical versus empirical secular change in zircon composition. *Earth Planet. Sci. Lett.* **554**, 116660 (2021).
23. Gardiner, N. J. et al. Building Mesoarchaean crust upon Eoarchaean roots: the Akia Terrane, West Greenland. *Contrib. Mineral. Petrol.* **174**, https://doi.org/10.1007/s00410-019-1554-x (2019).
24. Olierook, H. K. H. et al. Regional zircon U-Pb geochronology for the Maniitsoq region, southwest Greenland. *Sci. Data* **8**, 139 (2021).
25. Stacey, J. S. & Kramers, J. D. Approximation of terrestrial lead isotope evolution by a two-stage model. *Earth Planet. Sci. Lett.* **26**, 207–221 (1975).
26. Garber, J. M., Hacker, B. R., Kylander-Clark, A. R. C., Stearns, M. & Seward, G. Controls on trace element uptake in metamorphic titanite: Implications for petrochronology. *J. Petrol.* **58**, 1031–1057 (2017).
27. Ribeiro, B. V. et al. From microanalysis to supercontinents: insights from the Rio Apa Terrane into the Mesoproterozoic SW Amazonian Craton evolution during Rodinia assembly. *J. Metamorph. Geol.* **40**, 631–663 (2021).
28. Olierook, H. K. H. et al. Unravelling complex geologic histories using U–Pb and trace element systematics of titanite. *Chem. Geol.* **504**, 105–122 (2019).
29. Scibiorski, E. A. & Cawood, P. A. Titanite as a petrogenetic indicator. *Terra Nova* **34**, 177–183 (2022).
30. Hayden, L. A., Watson, E. B. & Wark, D. A. A thermobarometer for sphene (titanite). *Contrib. Mineral. Petrol.* **155**, 529–540 (2008).
31. Rösel, D. & Zack, T. LA-ICP-MS/MS single-spot Rb-Sr dating. *Geostand. Geoanal. Res.* **46**, https://doi.org/10.1111/ggr.12414 (2022).
32. Jenkin, G. R. T., Ellam, R. M., Rogers, G. & Stuart, F. M. An investigation of closure temperature of the biotite Rb-Sr system: the importance of cation exchange. *Geochim. Cosmochim. Acta* **65**, 1141–1160 (2001).
33. Blanckenburg, F., Villa, I. M., Baur, H., Morteani, G. & Steiger, R. H. Time calibration of a PT-path from the Western Tauern Window, Eastern Alps: the problem of closure temperatures. *Contrib. Miner. Petrol.* **101**, 1–11 (1989).
34. Glodny, J., Kühn, A. & Austrheim, H. Diffusion versus recrystallization processes in Rb-Sr geochronology: Isotopic relics in eclogite facies rocks, Western Gneiss Region, Norway. *Geochim. Cosmochim. Acta* **72**, 506–525 (2008).
35. Eberlei, T. et al. Rb/Sr isotopic and compositional retentivity of muscovite during deformation. *Lithos* **227**, 161–178 (2015).
36. Allaart, J. H., Friend, C. R. L., Hall, R. P., Jensen, S. B. & Roberts, I. W. N. Continued 1:500 000 reconnaissance mapping in the Precambrian of the Sukkertoppen region, southern West Greenland. *Rapport Grønlands Geologiske Undersøgelse* **90**, 50–54 (1978).
37. Cherniak, D. J. Lead diffusion in titanite and preliminary results on the effects of radiation damage on Pb transport. *Chem. Geol.* **110**, 177–194 (1993).
38. Holder, R. M., Hacker, B. R., Seward, G. G. E. & Kylander-Clark, A. R. C. Interpreting titanite U–Pb dates and Zr thermobarometry in high-grade rocks: empirical constraints on elemental diffusivities of Pb, Al, Fe, Zr, Nb, and Ce. *Contrib. Mineral. Petrol.* **174**, 42 (2019).
39. Cherniak, D. J. Sr and Nd diffusion in titanite. *Chem. Geol.* **125**, 219–232 (1995).
40. Levsky, L. K., Morozova, I. M., Levchenkov, O. A., Baikova, V. S. & Bogomolov, E. S. Isotopic-geochronological systems in metamorphic rocks: Pon'goma Island, Belomorian mobile belt. *Geochem. Int.* **47**, 215–230 (2009).
41. Hickman, M. H. & Glassley, W. E. The role of metamorphic fluid transport in the Rb-Sr isotopic resetting of shear zones: evidence from Nordre Strømfjord, West Greenland. *Contrib. Mineral. Petrol.* **87**, 265–281 (1984).
42. Müller, S. et al. Age and temperature-time evolution of retrogressed eclogite-facies rocks in the Paleoproterozoic Nagssugtoqidian Orogen, South-East Greenland: constrained from U-Pb dating of zircon, monazite, titanite and rutile. *Precambrian Res.* **314**, 468–486 (2018).
43. Whitehouse, M. J., Kalsbeek, F. & Nutman, A. P. Crustal growth and crustal recycling in the Nagssugtoqidian orogen of West Greenland: constraints from radiogenic isotope systematics and U–Pb zircon geochronology. *Precambrian Res.* **91**, 365–381 (1998).
44. Henriksen, N., Higgins, A. K., Kalsbeek, F. & Pulvertaft, T. C. R. Greenland from archaean to quaternary. Descriptive text to the 1995 geological map of Greenland, 1:2 500 000. *GEUS Bull.* **18**, 1–126, (2009).
45. Kolb, J. Structure of the Palaeoproterozoic Nagssugtoqidian Orogen, South-East Greenland: model for the tectonic evolution. *Precambrian Res.* **255**, 809–822 (2014).
46. Nutman, A. P., Kalsbeek, F. & Friend, C. R. L. The nagssugtoqidian orogen in Souh-East Greenland:Evidence for paleoproterozoic collision and plate assembly. *Am. J. Sci.* **308**, 529–572 (2008).
47. Bridgwater, D. & Myers, J. S. Outline of the Nagssugtoqidian mobile belt of East Greenland. *Rapp. Gronlands Geol. Unders*., 9–18 (1979).
48. Connelly, J. N., Thrane, K., Krawiec, A. W. & Garde, A. A. Linking the Palaeoproterozoic Nagssugtoqidian and Rinkian orogens through the Disko Bugt region of West Greenland. *J. Geol. Soc.* **163**, 319–335 (2006).
49. Kalsbeek, F., Bridgwater, D. & Boak, J. Evidence of mid-Proterozoic granite formation in the Isua area. *Rep. Geol. Surv. Greenland* **100**, 73–75 (1980).
50. Garde, A. A., Larsen, O. & Nutman, A. P. Dating of late Archaean crustal mobilisation north of Qugssuk, Godthåbsfjord, southern West Greenland. *Rep. Geol. Surv. Greenland* **100**, 73–75 (1986).
51. Van Gool, J. A. M., Connelly, J. N., Marker, M. & Mengel, F. C. The Nagssugtoqidian Orogen of West Greenland: tectonic evolution and regional correlations from a West Greenland perspective. *Canadian J. Earth Sci.* **39**, 665–686 (2002).
52. Willigers, B. J. A., van Gool, J. A. M., Wijbrans, J. R., Krogstad, E. J. & Mezger, K. Posttectonic cooling of the nagssugtoqidian orogen and a comparison of contrasting cooling histories in precambrian and phanerozoic orogens. *J. Geol.* **110**, 503–517 (2002).
53. Garde, A. A., Windley, B. F., Kokfelt, T. F. & Keulen, N. Archaean plate tectonics in the North Atlantic Craton of West Greenland revealed by well-exposed horizontal crustal tectonics, Island Arcs and tonalite-trondhjemite-granodiorite complexes. *Front. Earth Sci.* **8** (2020).
54. Chew, D. M., Petrus, J. A. & Kamber, B. S. U-Pb LA-ICPMS dating using accessory mineral standards with variable common Pb. *Chemical Geology* **363**, 185–199 (2014).
55. Whitehouse, M. J., Myers, J. S. & Fedo, C. M. The Akilia controversy: field, structural and geochronological evidence questions interpretations of >3.8 Ga life in SW Greenland. *J. Geol. Soc.* **166**, 335–348 (2009).
56. Friend, C. R. L. & Nutman, A. P. Two Archaean granulite-facies metamorphic events in the Nuuk- Maniitsoq region, southern West Greenland: correlation with the Saglek block, Labrador. *J. Geol. Soc.* **151**, 421–424 (1994).
57. Windley, B. F. & Garde, A. A. Arc-generated blocks with crustal sections in the North Atlantic craton of West Greenland: crustal growth in the Archean with modern analogues. *Earth-Sci. Rev.* **93**, 1–30 (2009).
58. Dyck, B., Reno, B. L. & Kokfelt, T. F. The Majorqaq Belt: a record of Neoarchaean orogenesis during final assembly of the North Atlantic Craton, southern West Greenland. *Lithos* **220-223**, 253–271 (2015).
59. Kirkland, C. L. et al. Widespread reworking of Hadean-to-Eoarchean continents during Earth's thermal peak. *Nature Communications* **12**, 331 (2021).
60. Waterton, P. et al. Geodynamic implications of synchronous norite and TTG formation in the 3 Ga Maniitsoq Norite Belt, West Greenland. *Front. Earth Sci.* **8** 562062 (2020).
61. Garde, A. A., Pattison, J., Kokfelt, T. F., McDonald, I. & Secher, K. The norite belt in the Mesoarchaean Maniitsoq structure, southern West Greenland: conduit-type Ni-Cu mineralisation in impact-triggered, mantle-derived intrusions? *GEUS Bull.* **28**, 45–48 (2013).
62. Ravenelle, J. F., Weiershauser, L. & Cole, G. Updated independent technical report for the maniitsoq nickel-copper-cobalt-PGM Project, Greenland. 3CN024.004 – North American Nickel Inc. (2017).
63. Garde, A. A., McDonald, I., Dyck, B. & Keulen, N. Searching for giant, ancient impact structures on Earth: the Mesoarchaean Maniitsoq structure, West Greenland. *Earth Planet. Sci. Lett.* **337-338**, 197–210 (2012).
64. Yakymchuk, C. et al. Stirred not shaken; critical evaluation of a proposed Archean meteorite impact in West Greenland. *Earth Planet. Sci. Lett.* **557**, 116730 (2021).
65. Kirkland, C. L. et al. Apatite and biotite thermochronometers help explain an Arctic Caledonide inverted metamorphic gradient. *Chem. Geol.* **584**, 120524 (2021).
66. Kirkland, C. L., Daly, J. S., Eide, E. A. & Whitehouse, M. J. Tectonic evolution of the Arctic Norwegian Caledonides from a texturally- and structurally-constrained multi-isotopic (Ar-Ar, Rb-Sr, Sm-Nd, U-Pb) study. *Am. J. Sci.* **307**, 459–526 (2007).
67. Ketcham, R. A. in *Techniques, Interpretations, and Applications* (eds Peter W. Reiners & Todd A. Ehlers) 275–314 (De Gruyter, 2005).
68. Kirkland, C. Supplementary material for "Dating mylonitic overprinting of ancient rocks". figshare. Collection. https://doi.org/10.6084/m9.figshare.c.5626387.v1 (2023).
69. Friend, C. R. L. & Nutman, A. P. Tectono-stratigraphic terranes in Archaean gneiss complexes as evidence for plate tectonics: the Nuuk region, southern West Greenland. *Gondwana Res.* **72**, 213–237 (2019).
70. McDonough, W. F. & Sun, S.-S. The composition of the Earth. *Chem. Geol.* **2541**, 223–253 (1995).
71. O'Neill, H. S. C. The smoothness and shapes of chondrite-normalized rare earth element patterns in Basalts. *J. Petrol.* **57**, 1463–1508 (2016).
72. Anenburg, M. & Williams, M. J. Quantifying the tetrad effect, shape components, and Ce–Eu–Gd anomalies in rare earth element patterns. *Math. Geosci.* **54**, 47–70 (2022).

Acknowledgements
The Mineral Resources Authority, Government of Greenland, is thanked for funding this research and providing access to sample material from its government collections. No additional sampling permissions are required. The GeoHistory Facility at the John de Laeter Centre, Curtin University, is supported by AuScope and the Australian Government. The authors also thank three anonymous reviewers and F. Corfu for insightful comments that greatly improved this contribution.

Author contributions
C.K. designed the study, wrote the original draft, and was responsible for data interpretation. H.O. performed sample imaging. J.L., B.R., and K.A. performed laser ablation analysis. M.D. performed thermal modeling. J.H. provided field sample context. All authors contributed to reviewing and editing this work.

Competing interests
The authors declare no competing interests.

Additional information
Supplementary information The online version contains supplementary material available at https://doi.org/10.1038/s43247-023-00709-5.

Correspondence and requests for materials should be addressed to Christopher L. Kirkland.

Peer review information *Communications Earth & Environment* thanks Fernando Corfu and the other, anonymous, reviewer(s) for their contribution to the peer review of this work. Primary Handling Editors: Derya Gürer and Joe Aslin. Peer reviewer reports are available.